

Article

Physical and Chemical Properties of *Pachycymbiola brasiliiana* Eggshells—From Application to Separative Processes

Martin A. Masuelli ^{1,*} , Lismet Lazo ¹, Federico Becerra ¹, Fernanda Torres ¹, Cristian O. Illanes ² , Andres Takara ², Maria Lujan Auad ³ and Maria Bercea ⁴ 

- ¹ Instituto de Física Aplicada-CONICET-UNSL, Laboratorio de Investigación y Servicios de Química Física, Área de Química Física, Departamento de Química, Facultad de Química, Bioquímica y Farmacia, Universidad Nacional de San Luis, Ejército de los Andes 950, San Luis D5700HHW, Argentina; lismeth38@gmail.com (L.L.); federicobecerra456@gmail.com (F.B.)
- ² Instituto de Física Aplicada-CONICET-UNSL, Laboratorio de Membranas y Biomateriales, Área de Tecnología Química y Biotecnología, Departamento de Química, Facultad de Química, Bioquímica y Farmacia, Universidad Nacional de San Luis, Ejército de los Andes 950, San Luis D5700HHW, Argentina; eatakara@gmail.com (A.T.)
- ³ Center for Polymers and Advanced Composites, Department of Chemical Engineering, Auburn University, Auburn, AL 36849, USA; mla0001@auburn.edu
- ⁴ “Petru Poni” Institute of Macromolecular Chemistry, 41-A Grigore Ghica Voda Alley, 700487 Iasi, Romania; bercea@icmpp.ro
- * Correspondence: masuelli@unsl.edu.ar or masuellimartin94@gmail.com

Abstract: *Pachycymbiola brasiliiana* is a marine snail found in the seas adjacent to the coasts of Brazil, Uruguay, and Argentina, whose eggshells are composed primarily of chitin. In this work, *Pachycymbiola brasiliiana* eggshells were used to prepare films and their structural and physicochemical characteristics were investigated. The main focus was on their mechanical stability, water sorption, and methylene blue rejection. From the FTIR spectra, the bands corresponding to chitin were identified. The differential scanning calorimetric (DSC) data showed that the biopolymer has a glass transition temperature of around 32 °C. The morphological analysis was carried out by using SEM and XRD. The study of the films’ mechanical stability showed an improvement with an increase in water activity. Regarding the methylene blue separation processes, a low permeation through the film and a rejection rate of 94 to 99% were demonstrated. Therefore, *Pachycymbiola brasiliiana* eggshell can be considered a promising source of biopolymers for preparing biodegradable, non-toxic films with valuable separative properties.

Keywords: *Pachycymbiola brasiliiana*; biopolymer; mechanical stability; water sorption; methylene blue separation



Citation: Masuelli, M.A.; Lazo, L.; Becerra, F.; Torres, F.; Illanes, C.O.; Takara, A.; Auad, M.L.; Bercea, M. Physical and Chemical Properties of *Pachycymbiola brasiliiana* Eggshells—From Application to Separative Processes. *Processes* **2024**, *12*, 814. <https://doi.org/10.3390/pr12040814>

Academic Editor: Angela Scala

Received: 11 March 2024

Revised: 15 April 2024

Accepted: 15 April 2024

Published: 18 April 2024



Copyright: © 2024 by the authors. Licensee MDPI, Basel, Switzerland. This article is an open access article distributed under the terms and conditions of the Creative Commons Attribution (CC BY) license (<https://creativecommons.org/licenses/by/4.0/>).

1. Introduction

Pachycymbiola brasiliiana (Lamarck, 1811), denoted as PBn, is a species of gastropod mollusk in the family Volutidae. The female of this species deposits an ovoid capsule (egg) measuring between 4 and 8 cm in diameter. This capsule is translucent and yellow, housing the development of 9 to 33 embryos. These embryos hatch into small snails approximately one centimeter in length, sustaining themselves by consuming the surrounding liquid. These capsules are not attached to the substrate; water currents can transport them, so they are expected to be found on sandy beaches along the coasts of Brazil, Uruguay, and Argentina [1–3].

The chicken eggshell is the most-common and -widely studied, mainly due to its availability. It is usually composed of ceramic-like materials consisting of a three-layer structure, namely, the cuticle on the outer surface, a spongy (calcareous) layer, and an internal lamellar (or mammillary) layer [4]. A study of the chemical and physical characterizations of the eggshell and eggshell membrane particles was released, which used material

prepared from hen eggshell waste as the methylene blue (MB) sorbent. [4]. Typically, chicken eggshells are highly rich in calcium (90%), with a small percentage (less than 5%) of phosphorus [5]. Chicken eggshells can be used as a raw material for dye removal, soil stabilization, ceramics [6], an adsorbent for the removal of heavy metals and dyes from aqueous solutions [7], in biomedical engineering [8], as a biotemplate for the synthesis of nanoparticles [9], etc.

Studies of *Rapana venosa* egg capsules collected from the Romanian coast of the Black Sea have obtained very promising results for the extraction of chitosan oligomers (molecular weight between 1.5 kg/mol and 3 kg/mol) with a deacetylation degree of 74–76%, using a basic medium and temperatures between 80 °C and 90 °C for 2 h, with yields between 4 and 7% [10,11]. Chitosan, with a deacetylation degree of 54.98%, has been extracted from snail shells originally from the north-central zone of Nigeria [12].

The avian eggshell has been studied as a membrane for different purposes, such as an antioxidant, anti-inflammatory, and antibacterial agent; and as a biomaterial used for immobilization, tissue engineering, and food packaging [13]. The components of avian eggshells are rigid membranes composed primarily of calcium carbonate (CaCO_3) (approximately 95%), and an organic matrix composed of proteins, glycoproteins, and proteoglycans (approximately 3.5%) [14].

Crustacean shells composed of chitin, which is an insoluble and linear biopolymer comprising 1,4-linked β -D-N-acetyl-glucosamine units, have been used for film-forming applications [15,16].

The production of membranes/films derived from biopolymers is garnering escalating interest owing to their distinctive and unparalleled characteristics, rendering them potentially the preferred option across a broad spectrum of applications. Research in membrane/film science is increasingly focusing on the possibility of using alternative polymers derived from natural raw materials to develop new membranes/films. Biopolymers can be produced from green and sustainable sources, such as microorganisms, plants, and animals, allowing for the realization of a growing circular economy [17].

Studies on the native eggshells of *Pachycymbiola brasiliiana* (Pbn) snails are very limited, so this work attempts to clarify and deepen their study using structural and other functional analyses. Pbn was physically and structurally characterized by FTIR, DRX, DSC, TGA-DTGA, SEM-EDX, colorimetric, solubility, and acetylation degree measurements. The films were also characterized by water contact angle measurements, water vapor permeation, water vapor sorption, swelling index, water and MB flow through the film, mechanical tests, and biodegradability.

2. Results

2.1. Degree of Acetylation, Solubility, and FTIR

Snail eggshells present with a chitin-like structure (Figure 1), with soft characteristics in humid conditions or when submerged in water, with a low solubility of 2.98% and an acetylation degree of 66.7%.

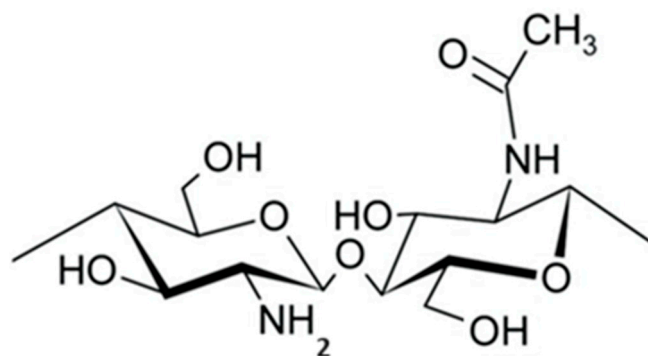


Figure 1. The chemical structure of chitin/chitosan.

FTIR accounts for the bands corresponding to the functional group of the material under study. The FTIR spectrum of the dry sample evidenced an aminopyranosic structure (Figure 2). According to the FTIR data, the -OH stretching frequency emerged at 3413 cm^{-1} . The CO (amide) and NH primary amine bands were observed at 1647 cm^{-1} and $2877\text{--}2871\text{ cm}^{-1}$ (CH_2 stretching), while the vibrational mode of amide $\text{C}=\text{O}$ stretching was observed at 1672 , and the NH primary amine bends were observed at 1647 cm^{-1} . The absorption bands at 1521 and 1396 cm^{-1} correspond to amide II (N-H bending) and amide III (C-N stretching), respectively [18]. The band at 1458 cm^{-1} was attributed to the C-H side-chain bending $-\text{CH}_2\text{OH}$. The band at 1232 cm^{-1} (C-O-C stretching) and the absorption band between 1220 and 1054 cm^{-1} represent the free amino group ($-\text{NH}_2$) at the glucosamine C2 position. The 1068 and 1054 cm^{-1} absorption peaks were assigned to C-O glucose bending. The peak at 771 cm^{-1} was ascribed to C-N stretching at 732 cm^{-1} (out-of-plane bending NH) and 561 cm^{-1} (out-of-plane bending NH, out-of-plane bending C-O) [10–16].

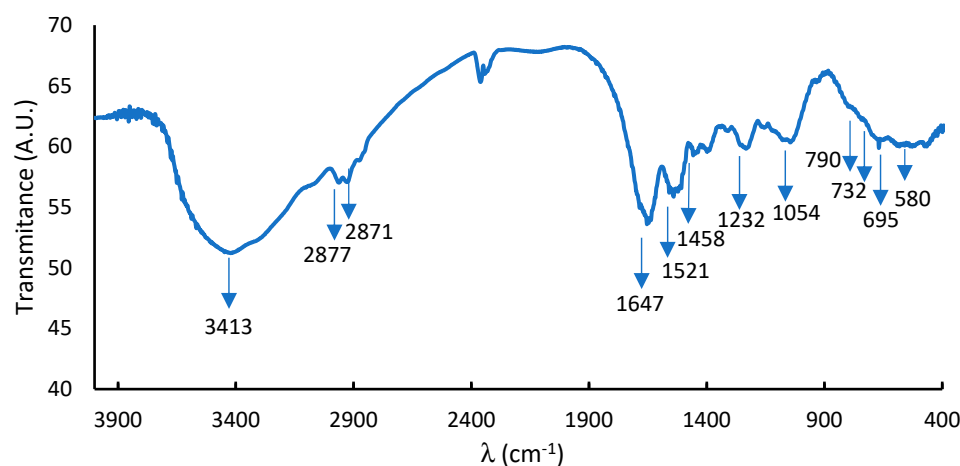


Figure 2. FTIR spectrum of PBn.

2.2. X-ray Diffraction (XRD)

X-ray diffraction accounts for the crystallinity of a material, and for a biopolymer it gives us information about the interchain spacing (d_{spacing}). PBn presents with two amorphous peaks at 2θ of 10.88° and 21.26° (Figure 3 and Table 1). The first is due to the inclusion of water within the crystal lattice, and the second is due to the low crystallinity typical of bonds with tighter d_{spacing} [19].

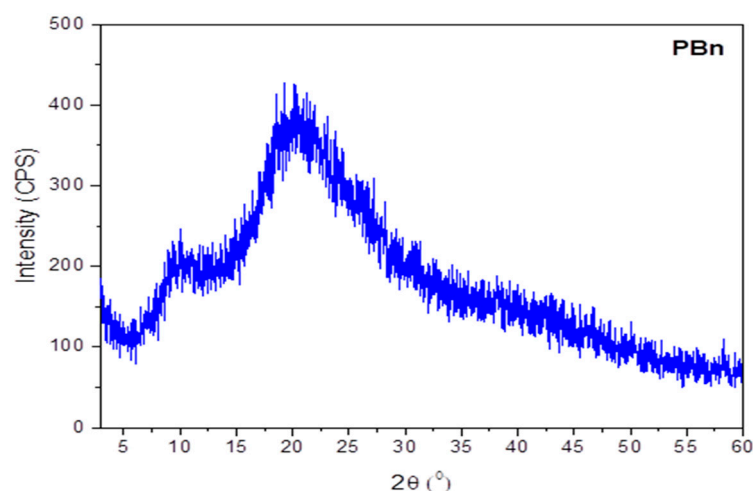


Figure 3. The XRD spectrum of PBn.

Table 1. XRD data for PBn.

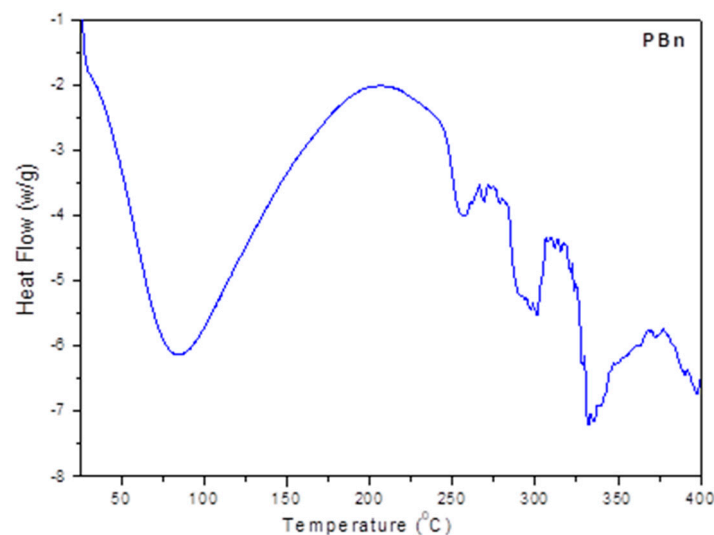
2θ	d_{spacing} (Å)
10.88	8.09
21.26	4.17

The crystallinity index is 43%, lower than those reported for α - or β -chitin extracted from crustaceans from the Arabian Gulf (Kuwait) [20]. In the same sense, α -chitin from crab shells [21] presents with a similarity in the ICr (crystallinity index), due to the degree of acetylation of 70% with an ICr value of 44, compared to the sample studied in the present work.

2.3. Differential Scanning Calorimetric Analysis (DSC)

Differential scanning calorimetry (DSC) is a thermoanalytical technique in which the heat difference between a sample and a reference is measured as a function of temperature, accounting for the different transition states of the sample.

The DSC analysis of PBn shows a glass transition temperature of 32 °C (Figure 4). PBn has an endothermic peak at 211 °C, corresponding to the melting temperature, similar to those reported for chitin films at 219 °C [22]. Above 250 °C, the polysaccharide chains begin to decompose [23].

**Figure 4.** DSC thermogram of PBn.

2.4. Thermogravimetric Analysis—Differential Thermal Analysis

The thermogravimetric analysis—differential thermal analysis (TGA-DTGA) performed on the PBn film with a heating rate of 10 °C/min shows the thermal characteristics of a polysaccharide (Figure 5). In this experiment, PBn underwent three stages of mass loss: (i) the water evaporation of PBn between 50 °C and 100 °C, (ii) the decomposition temperature was measured to be at 250 °C, and (iii) it finished at 400 °C. During the decomposition process, the PBn chains begin to degrade and, finally, the biopolymer matrix completely decomposes at 330 °C [24–26].

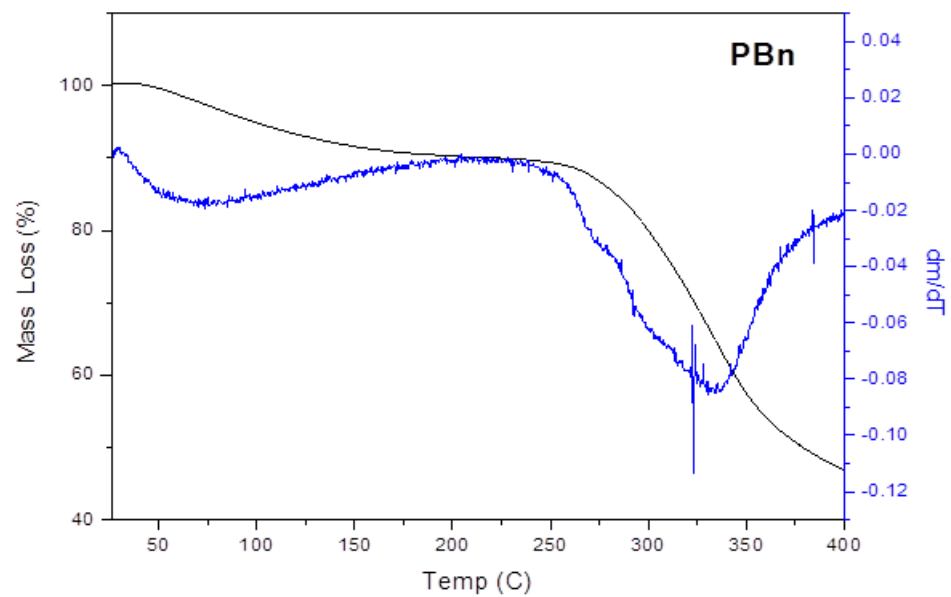


Figure 5. TGA-DTGA curves of PBn.

These results are in agreement with the literature data [24–26]; above 250°, the thermal stability of a polysaccharide is affected by decomposition (see Figure 5).

2.5. Scanning Electron Microscopy–Electron and Dispersive X-ray Spectroscopy (SEM-EDX)

This SEM technique accounts for the surface morphology of the film and the EDX determines the number of elements that compose it. According to the SEM observations, the surface of the film is rough, with regular indentations of a similar size between 0.2 and 0.7 μm long by approximately 0.1 μm wide (see Figure 6). Chitin whiskers indicate the surface uniformity of the film as significantly improved, and display a smooth and dense structure [27–29].

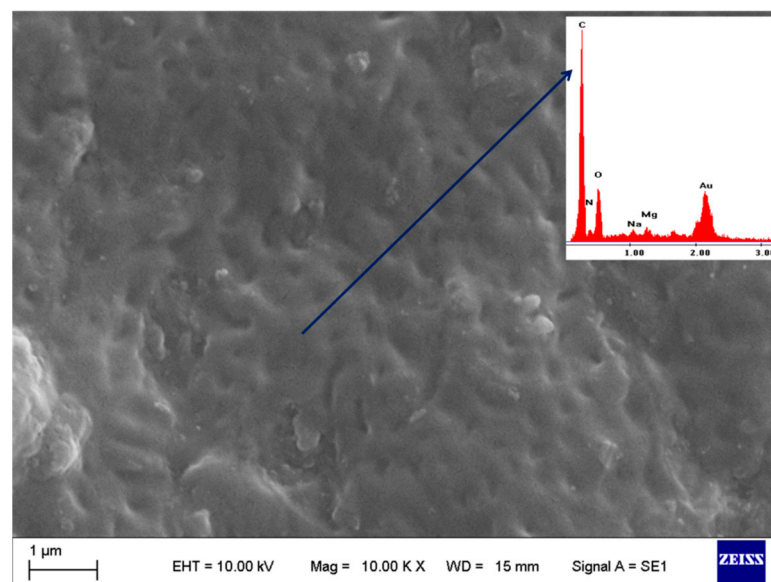


Figure 6. SEM image and EDX analysis of PBn surface. The blue arrow points to the section where the EDX was measured.

The EDX analysis shows the presence of C, O, and N distributed uniformly within the membrane. Also, elements such as Na and Mg appear in the PBn samples.

2.6. Colorimetry

Colorimetry essentially consists of adding the response to colored stimuli and its normalization to the spectral response curve of the color-sensitive photoreceptor. From Table 2, it can be seen that the PBn colors are typically light brown. The dry films are more transparent than the wet films (<https://www.e-paint.co.uk/convert-lab.asp>, accessed on 1 December 2023).

Table 2. Colorimetric analysis of dry/wet PBn.

	L*	a*	b*	Online Color	Real Color
PBn Dry	59.09	0.91	23.70		
PBn Wet	67.23	4.45	13.33		

The sorption of water within the PBn structure achieves a color change because hydrogen bonds are generated that change its structure.

2.7. Mechanical Test

The tensile test (mechanical test) of a material consists of subjecting a standardized specimen to an increasing axial tensile stress until it breaks. This test measures the resistance of a material to a static force. Previous studies [24,25] have shown that films' tensile stress–strain curves present a fine correlation between the breaking stress and strain for a humid sample.

According to Figure 7 and Table 3, when the humidity of the film increases, the maximum tensile stress decreases, but the maximum shear stress increases notably. Young's modulus decreases noticeably when the humidity of the film increases.

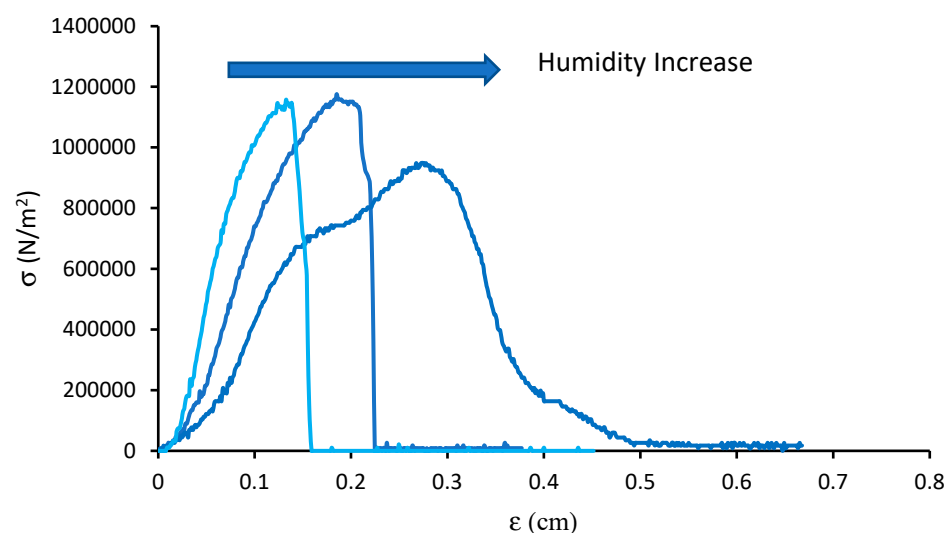


Figure 7. Mechanical test of PBn samples with different humidities.

Table 3. Mechanical data obtained for PBN samples with different humidities.

RH (%)	ϵ (%)	σ (MPa)	E (MPa)
10	13.75	11.5	14.8
30	20.31	11.4	9.06
50	29.65	0.93	5.43

Glycerol and water are used as plasticizers in film formulations, improving the mechanical stability of PBN membranes. Plasticizers are commonly used to facilitate processing and/or to increase the material's flexibility. Water, some oligosaccharides, polyols, and lipids are different types of plasticizers widely used in hydrocolloid-based films. Their combination could give rise to synergistic effects between the components, considerably improving the properties of the films or hydrogels. Various theories have been proposed to explain the actions of these compounds. For example, lubrication theory postulates that the plasticizers intermix and act as internal lubricants by reducing the friction forces between the polymer chains. The gel theory assumes that the rigidity of the polymer network comes from its three-dimensional structure, so the plasticizers act by breaking the polymer–polymer interactions, that is, by interposing themselves between the macromolecular chains. The free volume theory considers the addition of plasticizers as a way to increase the free volume, reducing the interactions between the chains [24–28].

2.8. Contact Angle

The contact angle refers to the angle that the surface of a liquid forms when it comes into contact with a solid. This value depends mainly on the relationship between the adhesive forces between the liquid and the solid surface and the cohesive forces of the liquid. Therefore, the contact angle accounts for the affinity of the liquid on the surface of the film, and whether the liquid wets or does not wet.

After waiting 30 s, a contact angle value of 41° was determined. This short time was used for the measurement since the biopolymer quickly absorbs the water molecules. The contact angle value obtained for the PBN film indicates hydrophilic behavior, but it was slightly lower than that of the commercial chitin sample, for which a contact angle of 31.05° has been reported [24]. This low contact angle could be due to the physical bonds and, in particular, to the hydrogen bonds, and its value explains the behavior of the PBN films in the presence of water molecules.

2.9. Water Vapor Permeability and Water Vapor Sorption

The water vapor sorption isotherm shows the equilibrium amount of vapor adsorbed at a constant temperature (Figure 8). An increase in mass can be observed due to the water vapor permeability, with a value of $3.74 \text{ ng m/m}^2 \text{ s Pa}$. This value is due to the PBN structure, which has a great affinity for water. This phenomenon is caused by the interaction between the hydrophilic groups of PBN and the water molecules, as observed during the initial step of water vapor sorption (during the first 30 min, see Figure 9).

Chitosan membranes crosslinked with glutaraldehyde exhibit high water sorption [19]. Similar results have been found for tragacanth–glutaraldehyde films [28]. According to Beppu et al. [19], chitosan ions decrease the permeability compared to crosslinked chitosan.

From a kinetic point of view, PBN water sorption displays three stages, similar to that of chemically crosslinked films [28]: the first stage (during the first 30 min of immersion in water), when the sorption phenomenon responds to the first-order kinetics; the intermediate step (between 30 min and 75 min), when the water sorption reaches equilibrium; and finally, the zero-order stage of desorption (for times longer than 75 min).

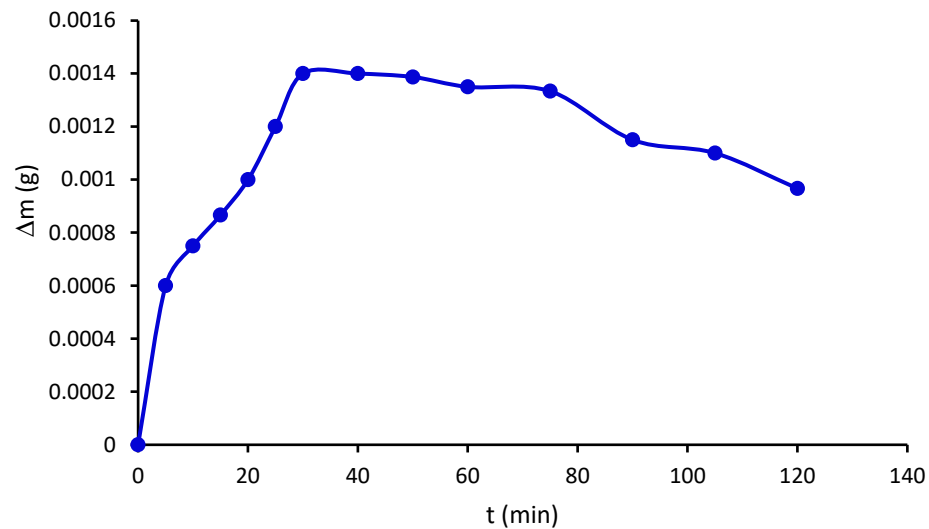


Figure 8. Water vapor sorption of PBn at a temperature of 30 °C.

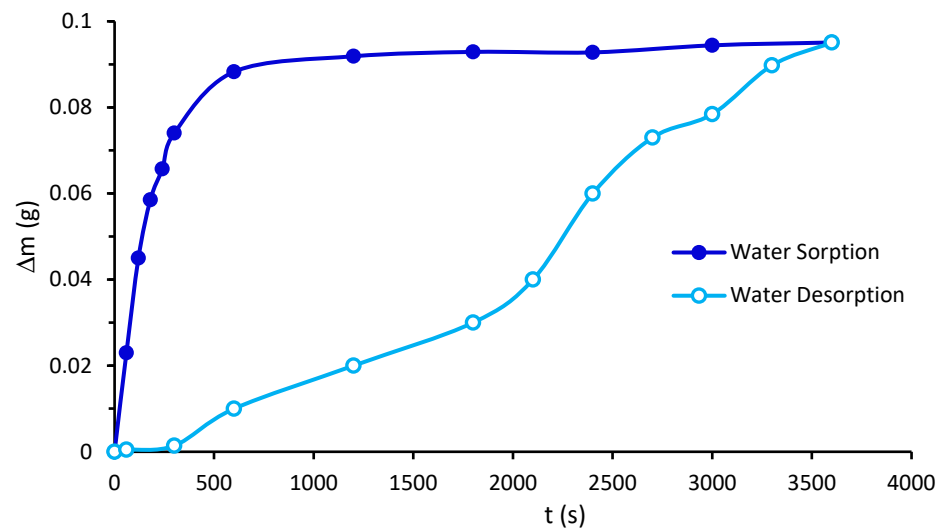


Figure 9. Swelling index of PBn (light blue—sorption, blue—desorption).

2.10. Swelling Index

Given the data on its great affinity for water and its stability as a film, PBn is a material whose macromolecules retain a large amount of water (Figure 9), a similar situation as that of chitosan [19]. In the case of alginate and chitosan bilayer membranes, they present with higher swelling index values compared to pure alginate and chitosan films [30]. PBn shows a great affinity for water, similar to films of chitin whiskers and sodium alginate/gelatin [23].

The water solubility of films made with biopolymers is an important property in packaging, since the films must maintain the necessary stability so that the packaged material has a long duration that increases its useful life [31].

2.11. Pure Water Flux and Methylene Blue Flux

Our permeability studies used the PBn films as a barrier between two sides: one side contained water or an MB aqueous solution, the other side accumulated the water and part of the MB passing through the membrane. The experimental results obtained for the pure water flux and MB flux through the PBn film are shown in Figures 10 and 11, respectively.

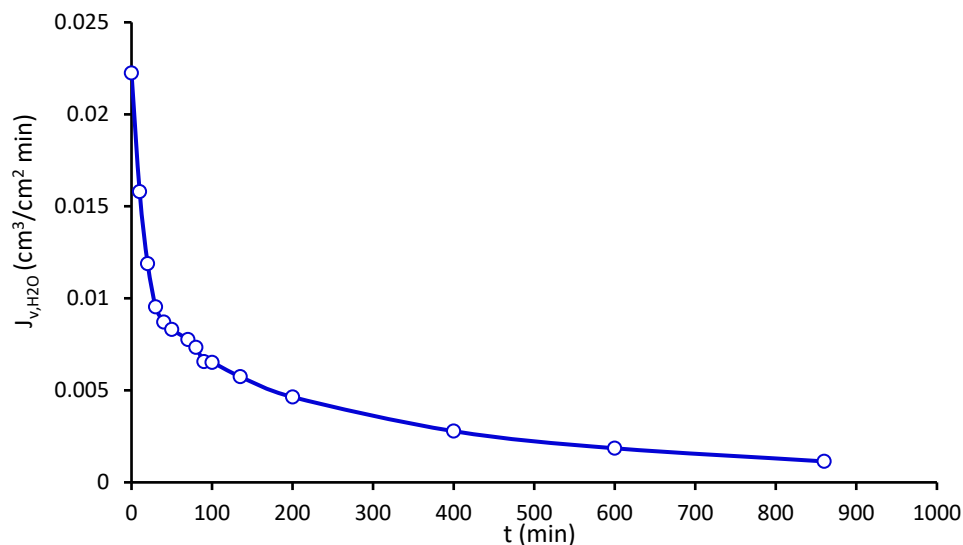


Figure 10. Water flux through PBN membrane.

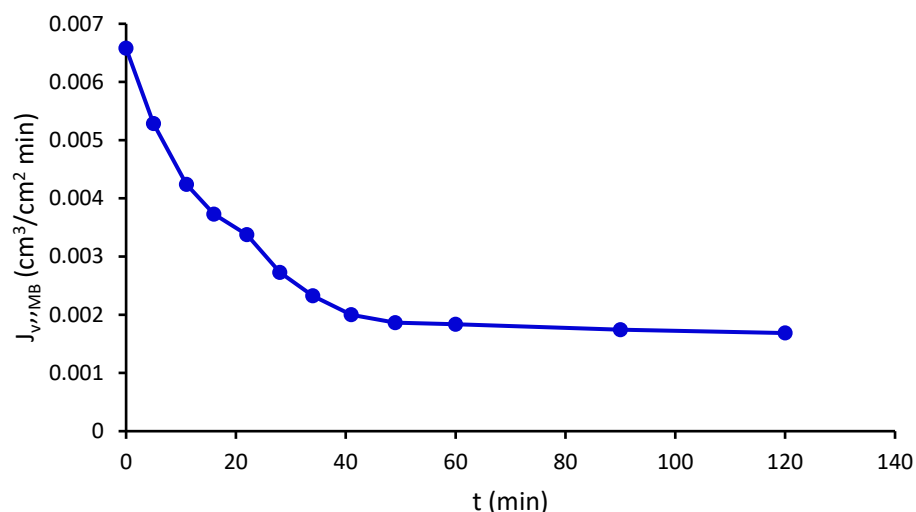


Figure 11. MB flux through PBN film.

The experiment for pure water flow (PWF) was carried out using the following operational data: temperature of 23 °C, pure water density of 0.99762 g/cm³, and water viscosity of 0.9321 cP. The pure water flow (PWF) through the PBN membrane is comparable to that of chitosan films; the PWF decreases with an increasing film thickness, as shown in reference [32]. This type of superhydrophilic film is helpful for water recovery from different effluents (see references [33–35]).

The fall in the MB permeate flux is mainly due to the accumulation of MB on the surface and inside of the PBN film (Figure 12). This may be due to MB's size-exclusion retention concerning the interchain spaces of PBN, with a d_{spacing} between 4.17 and 8.04 nm, accompanied by a strong interaction between the functional groups of PBN and MB.

For example, thin-film composite membranes of nano-clay (Cloisite 15A and 30B)/chitosan nanocomposite coated on a commercial poly(vinylidene fluoride) (PVDF) microfiltration membrane have good MB retention [33]. However, cellulose–chitosan biopolymer blend membranes have good rejection of oil/water emulsions [36] and metal wastewater treatment [37].

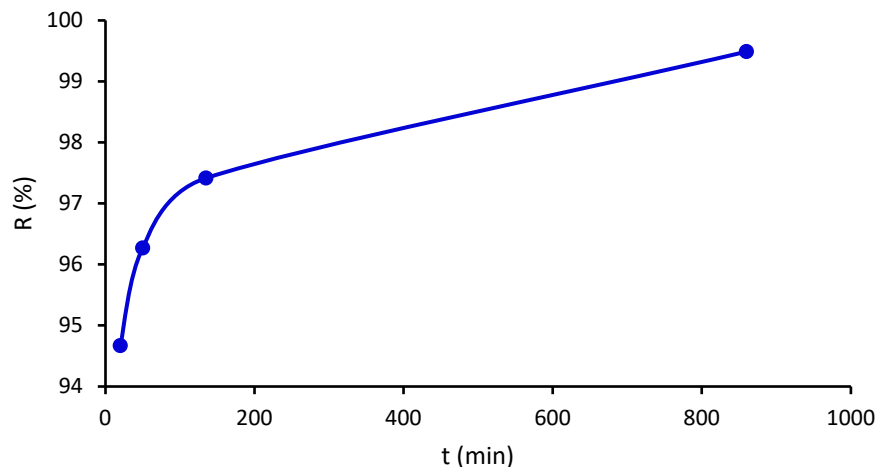


Figure 12. MB rejection of PBN.

The ZnO–chitosan nanocomposites have a high MB retention [38]. After five adsorption cycles, poly(acrylic acid)/chitosan-*g*-polyvinylamine hydrogels removed above 85% of MB [39]. Nanofiber membranes of chitosan, poly(vinylpyrrolidone), and poly(vinyl alcohol) prepared by electrospinning have shown promising potential for water purification, removing 83.91% of MB [40]. A polyethersulfone/chitosan composite-based ultrafiltration membrane presented with an MB rejection of 97.34% [41].

In this work, the MB rejection amount is between 94% and 99%, which shows that PBN is a suitable material for MB removal from waste water (Figure 13). The rejection of MB may be due to two combined phenomena, the first a simple size exclusion and the second the great affinity of PBN for water. Although the exclusion due to size is not total, since the membrane allows for the passage of some MB molecules, these molecules accumulate in the pores and end up excluding it. The formed cake only allows for the passage of the MB molecules and not of water ones, because the PBN material is hydrophilic.

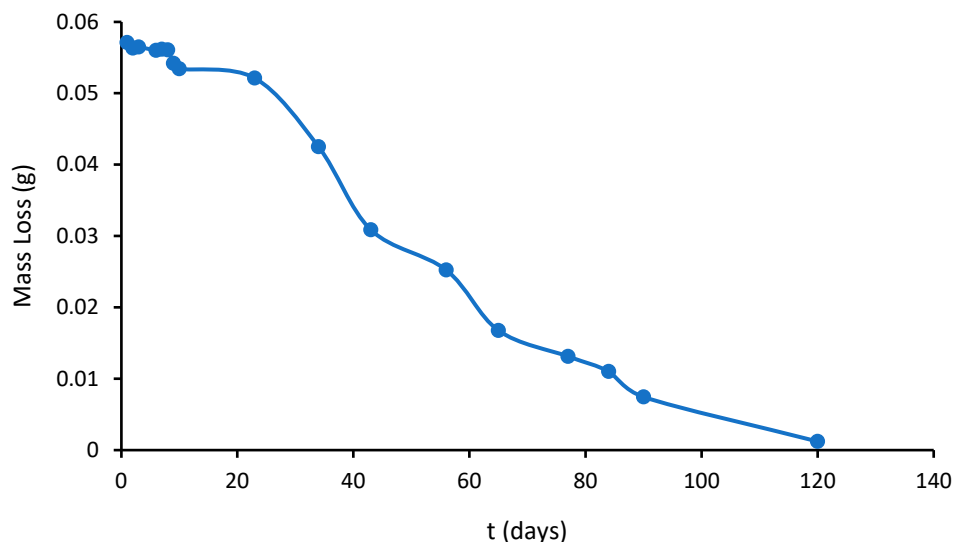


Figure 13. Biodegradability test of PBN film.

2.12. Biodegradability

Biodegradability is the ability of a material to be decomposed; therefore, it is a natural process in which a material, due to microbiological action, changes by degrading. In general, the material loses its original properties and, chemically, the molecules become simpler and more stable. Over a total period of 120 days, the biodegradation of PBN occurred in several stages, i.e., initial degradation, intermediate plateau, and final (total) degradation (Figure 13).

In the initial stage, microorganisms start the material's degradation with a rapid mass loss during the first days. Then, from day 10 to day 45, a plateau stage is reached with an almost constant weight (intermediate stage), when the PBn biodegradation rate is nearly zero. After 45 days, during the last stage, the mass decreases significantly until total degradation takes place (day 90). Generally, the biodegradation of chitin and chitosan occurs over 25 days or more [42–44].

3. Materials and Methods

3.1. Raw Material

PBn eggs were collected from the coast of Santa Teresita, Buenos Aires Province, Argentina. These eggshells were washed with plain water to remove all the sand, then with distilled water and, finally, dried at 60 °C for 24 h. For the mechanical tests, the eggshells were rehydrated by immersing them in distilled water; then, specimens were cut 4 cm long by 1 cm wide, and their thickness was measured with a micrometer. The contact angle, water vapor permeability, water vapor sorption, and swelling index cells were wet cut into 1 cm diameter circles; the thickness was also measured for each case. These film pieces were dried at room temperature between glass plates to retain their shape.

3.2. Degree of Acetylation

The acetylation degree (AD) measurement was performed using the acid–base titration method reported by Domard and Rinaudo in 1983 [45], with some alterations. An amount of 0.25 g of PBn samples was dissolved in 30 mL of HCl (0.1 mol/L), followed by stirring for 50 min to dissolve the PBn and cooling at 24 °C. Then, 5 to 6 drops of methyl orange were added to the suspension. The PBn dispersion was titrated against NaOH (0.1 mol/L) until the color turned from red to orange [45]. The AD% was calculated as follows.

$$AD\% = \left(\frac{(VN)_{HOtit} - (VN)_{HOBlank}}{(VN)_H} \right) \frac{0.25}{PM_{monomer}} 1000 \times 100 \quad (1)$$

where $(VN)_{HOtit}$ is the titrated volume for normality of NaOH 0.1 M, $VN_{HOBlank}$ is the blank volume for normality, $(VN)_H$ is the volume for normality of HCl 0.1 M, and $PM_{monomer}$ is the glucosamine molecular weight.

3.3. Solubility

For the solubility of PBn, 0.1 g of the sample was weighted and dispersed in acetic acid (40% vol., 10 mL) with the help of a magnetic stirrer (300 rpm at 25 °C for 60 min). Further, the suspension was submerged in a boiling water bath for 10 min and cooled at 25 °C. The undissolved particles were separated and washed in distilled water and dried at 60 °C for 24 h. The dried particles were weighed and the solubility was calculated using the following equation [46,47]:

$$S\% = \left(\frac{W_2 - W_1}{W_2} \right) 100 \quad (2)$$

where W_1 is the weight (g) of the insoluble PBn, and W_2 is the total weight (g) of the PBn.

3.4. Fourier Transform Infrared Spectroscopy

FTIR spectra were determined using diffuse reflectance (DRIFTS) and the transmission mode using a Nicolet PROTEGE 460 Spectrometer (Praga, R. Checa). The operational range was from 700 to 4000 cm^{-1} . The number of scans for each sample was 64 [48].

3.5. X-ray Diffraction (XRD)

X-ray diffraction (XRD) studies were carried out using Rigaku equipment, model ULTIMA IV type II (Tokyo, Japan), with a Cu K_α lamp ($\lambda_B = 1.54 \text{ \AA}$) and a nickel filter.

The 2θ operational range was from 3° to 60° , operated at 30 kV, 20 mA, with a 3° per minute sweep rate, 0.02° reading step, and continuous mode. The $d_{spacing}$ was determined by Bragg's equation.

$$d_{spacing} = \frac{n \lambda_B}{2 \sin \theta_B} \quad (3)$$

where $d_{spacing}$ is the average intercatenary distance, n is the integer determined, λ_B is the X-ray wavelength, and θ_B is Bragg's angle [49].

The crystalline index (IC_R) was calculated from the normalized diffractogram using the intensities of the peaks at 110 lattices (I_{max} , at $2\theta \cong 21^\circ$ corresponding to maximum intensity), and the I_{ad} at $2\theta \cong 15^\circ$ (amorphous diffraction) was used to calculate IC_R , as performed in [50,51].

$$IC_r = 100 \frac{I_{max} - I_{ad}}{I_{max}} \quad (4)$$

3.6. Differential Scanning Calorimetric Analysis (DSC)

Differential scanning calorimetry (DSC) was obtained using STA 449F3-Jupiter equipment (Selb, Germany). Approximately 5 mg of the PBN sample was placed in an alumina crucible, and the sample was heated from 25 to 400°C ; the heating ratio was $5^\circ\text{C}/\text{min}$ under a dynamic nitrogen atmosphere with a flow of 25 mL min^{-1} [49].

3.7. Thermogravimetric Analysis—Differential Thermogravimetric Analysis

The thermal stability of the PBN films was determined with a thermogravimetric analysis (TGA). The TGA determinations were conducted on a TG 2950 analyzer (TA Instruments, Inc., New Castle, DE, USA). The operating conditions were a heating rate of $10^\circ\text{C}/\text{min}$ in a N_2 (99.99%) atmosphere with a flow rate of $50 \text{ mL}/\text{min}$, which was previously microfiltered. The thermogravimetric temperature axes were calibrated with indium (99.99%, melting point of 156.60°C) and the Curie point of Ni (353°C), respectively. Empty aluminum pans (40 mL) were used as references. Polysaccharide samples of about 8 mg were employed [49].

3.8. Scanning Electron Microscopy—Electron Dispersive X-ray Spectroscopy (SEM-EDX)

The films' morphology was analyzed using an SEM, LEO 1450VP (Los Altos, CA, USA), and the energy dispersion X-ray analysis was performed using an EDS Genesis 2000 (EDAX, Los Altos, CA, USA). The samples for the SEM surface analysis were prepared by immersion in liquid nitrogen and, afterward, coated with gold. The PBN samples were observed under a high vacuum, and the EDAX spectrums were obtained by applying an acceleration voltage of 120 kV [49].

3.9. Colorimetry

The equipment used for the colorimetry was a MiniScan EZ (Reston, VI, USA), model MSEZ-4500L with illuminant D65, observer 10, and geometry 45/0. A colorimeter determines the opacity and color index. The values measured by the equipment are given using the coordinates of the CIELAB color space. Color measurements were made for each PBN film (diameter of 2.5 cm) with the intermediate viewing area accessory. Three measurements were made at different points of the samples and the average values were recorded as the color parameters L^* , a^* , and b^* [49], where L^* indicates the luminosity from 0 (black) to 100 (white), and a^* and b^* are chromatographic coordinates, with a^* from green (+60) to red (+60), and b^* from blue (+60) to yellow (+60) [52]. The color image was evaluated according to <https://www.e-paint.co.uk/convert-lab.asp>, accessed on 1 December 2023.

3.10. Mechanical Tests

The mechanical properties were measured with a Brookfield CT3 (USA) instrument, according to the ASTM D882 requirements, at a constant traction speed of $0.1 \text{ mm}/\text{min}$. The experimental procedure for the mechanical properties was measured at a temperature of

25 °C and relative humidity of 40%. The test was carried out in triplicate. The test samples were 40 mm long by 10 mm wide, and the thickness was measured with a micrometer for each film. The force (F) and deformation (Δl) data were recorded until the breaking point. The tensile strength (σ) was calculated by dividing the maximum load by the specimen's initial cross-sectional area (A). The percentage elongation at break (% ϵ) was calculated as the change, as a percentage, from the initial length of the specimen ($l_0 = 40$ mm) at the point of sample failure. Finally, the elastic modulus, or Young's modulus (E), was determined from the slope of the stress (σ) vs. strain (ϵ) curve in the elastic region (the linear part of the curve) [48,49].

$$E = \frac{\sigma}{\epsilon} \quad (5)$$

$$\sigma = \frac{F}{A} \quad (6)$$

$$\epsilon = \frac{\Delta l}{l_0} \quad (7)$$

3.11. Contact Angle

The contact angle is a function of the liquid's surface tension and the substrate's surface free energy. It can be measured by placing a drop of a pure liquid on a solid surface. The angle formed between the solid/liquid interface and the liquid/vapor interface, whose vertex is where the three interfaces meet, constitutes the contact angle. The Young equation, below, describes the interactions between the adhesion and cohesion forces; from this equation, the surface energy per unit area can be calculated [48].

$$\gamma^{sv} = \gamma^{sl} + \gamma^{lv} \cos \theta \quad (8)$$

where θ is the contact angle, γ^{sv} is the surface tension of the solid/vapor inter-phase, γ^{sl} is the surface tension of the solid/liquid interface, and γ^{lv} is the surface tension of the liquid/vapor interface.

The films were placed on a smooth surface, and 0.1 cm³ of distilled water was deposited onto them. The height (h) of the drops, with a Vernier caliper, was measured after 1 min.

$$h = h_1 - h_0 \quad (9)$$

where h_1 is the drop height, and h_0 is the surface height (cm).

When the liquid wets and spreads on the surface of the membrane, the contact angle is between 0° and 90° and the appropriate ratio is

$$\theta = \arccos \left(1 - \sqrt{\frac{Bh^2}{1 - \frac{Bh^2}{2}}} \right) \quad (10)$$

When the liquid does not wet, the contact angle is greater than 90°, and the relationship is

$$\theta = \arccos \left(-1 + \sqrt{\frac{4 - 2Bh^2}{Bh^2}} \right) \quad (11)$$

where $B = \rho g / 2\gamma$, g is the acceleration of gravity (9.81 m/s²), ρ is the water density (g/cm³), and γ is the water interfacial tension (71.97 g/s²) [48].

3.12. Water Vapor Permeability

The equipment used for determining water vapor permeability was an Electrotech Systems, Chicago, IL, USA, which works as a closed system controlled by sensors for temperature and humidity measurements. The weight change was obtained by a RADWAG balance (Radom, Poland), with a precision of 0.1 mg, and a Köfke thickness micrometer (Munich, Germany), with an accuracy of 0.1 m. PBN samples of 25 mm in diameter were

cut, their thicknesses were measured, and they were placed in the perforated caps of the bottles with 20 g of silica gel inside each one. Each bottle with silica gel was weighed and the cap was put on before starting the experiment. Then, they were placed in the equipment, which must be at 30 °C and 85% humidity, and during the first hour, they were weighed every 5 min. Then, the weight of the bottles was measured every 15 min until the 3rd hour of the experiment, when it was measured at 1 h intervals until 24 h (ASTM E96).

The mechanism can be described for a homogeneous polymer film of thickness, permeant pressure p (with $p_1 > p_2$), and permeant concentrations c throughout the film (with $c_1 > c_2$):

$$\tau = \frac{Q}{t A} \quad (12)$$

$$P = \frac{\lambda}{\Delta P} \tau \quad (13)$$

where τ is the transmission speed (ng/m²s), Q is the permeating mass (ng), λ is the thickness of the film (m), A is the area of the cell (m²), t is the measurement time (s), and ΔP is the pure water vapor pressure (4238.605 Pa) [48,49,53].

3.13. Water Vapor Sorption

The determination of water sorption was carried out by weighing the PBn film (m_0), which was placed in the humidity chamber set at 90% and 30 °C, and measured at different times (m) [48] according to the following equation:

$$\Delta m = 100 \left(\frac{m - m_0}{m_0} \right) \quad (14)$$

3.14. Swelling Index

The swelling index (SI) measures the weight of the samples submerged in a bath of distilled water. As time advances, the swelling increases, manifesting itself in an increase in length, thickness, and weight, until equilibrium is achieved. Due to this increase in hydrophobicity, the time necessary to reach equilibrium is less. Each sample's weight (P , in grams) was measured every 30 min until equilibrium was reached. The subscript "0" indicates the initial measurement of each one. The data obtained from the SI test were used to calculate the amount of absorbed water [48]:

$$SI(\%) = 100 \left(\frac{p}{p_0} - 1 \right) \quad (15)$$

3.15. Pure Water Flux and Methylene Blue Flux

The flow of pure water through the film at an ambient pressure of 93.17 kPa and a temperature of 23 °C was obtained with the following equation [38,49–51]:

$$J_{v, H_2O} = \frac{w}{\rho A t} \quad (16)$$

where J_{v, H_2O} is the pure water flux (cm³/cm² min), w (g) is the mass of pure water permeated through the PBn film [54–56], ρ is the density of water (g/cm³), A is the area of the hemisphere (cm²), and t is the unit of elapsed time (min).

The MB solution was 0.001 M, and the MB density was 0.99812 g/cm³; the $J_{v, MB}$ was the MB flux through the PBn of the membrane or film.

The MB rejection percent was measured by UV-visible spectroscopy; the equipment used was a Genesys 10 UV, Thermo Scientific USA, at 664.5 nm, according to the following equation [54–56]:

$$R\% = 100 \left(\frac{A_{0.001} - A_{MB}}{A_{0.001}} \right) \quad (17)$$

$A_{0.001}$ is the absorbance of the MB solution at 0.001 M (corrected by dilution 1/10), and A_{MB} is the MB solution permeation.

3.16. Biodegradability

Biodegradation is the deterioration and transformation that happens in a biopolymer due to the action of enzymes and/or microorganisms, such as bacteria, yeasts, and fungi. Biodegradation can be total or partial. Partial biodegradation consists of the alteration of the chemical structure of a material and the loss of specific properties. The total biodegradation of a material means that it is completely consumed by microorganisms' actions, with methane (under anaerobic conditions) or CO₂ production (under aerobic conditions). A covered container was filled with approximately 1 kg of moistened soil sample at 85% RH. Samples 40 mm long by 10 mm wide were cut and buried 2 cm deep. The temperature used was 30 °C (mesophilic conditions) in a closed system. The weight and size of the samples were monitored periodically over a 120-day incubation period [48,49].

4. Conclusions

Pachycymbiola brasiliiana (PBn) eggshells were used to prepare versatile biofilms for efficient water purification. PBn contains mainly chitin, with a degree of crystallinity of about 43%, and interchain spacing of approximately 4–8 nm. The material is thermally stable up to 250 °C, having a glass transition temperature of around 32 °C.

PBn is a material that absorbs a large amount of water at equilibrium. In a dehydrated state, PBn is very brittle, but, as water sorption increases, it becomes more efficient at the removal of methylene blue (MB). The MB rejection amount is about 94–99%, which shows that PBn is a suitable material for MB removal from waste water.

Native PBn is a natural and economical product, used for the preparation of films without any modification. It has extraordinary properties in terms of sorption and permeation, since it has a great affinity for water, evidenced by studies of water permeation through the PBn membrane. This biomaterial has broad applicability to separative processes, and thereby possesses greater potential and advantages than chemically modified and purified materials. Future studies will highlight the ability of PBn to remove other pollutants from waste water.

Author Contributions: Methodology, L.L.; Formal analysis, F.B. and C.O.I.; Investigation, A.T.; Data curation, F.T.; Writing—original draft, M.A.M.; Writing—review and editing, M.L.A. and M.B. All authors have read and agreed to the published version of the manuscript.

Funding: PICT-2020-SERIEA-00895 (RAICES). Title: “Obtención de Polisacáridos a partir de Vegetales y Microorganismos de la Región del Semiárido de San Luis. Aplicaciones: Alimentarias, Geles y Bioempaque”, 2. PROICO 2-2918, UNSL: “Extracción y Caracterización de Polisacáridos naturales con potencial uso en Biotecnología” and 3. PIP 2021/2023, IF-2021-85081432-APN-DCP#CONICET, “Valorización biotecnológica de efluentes de destilería para la obtención de productos microbianos”.

Data Availability Statement: No new data were created or analyzed in this study. Data sharing is not applicable to this article.

Acknowledgments: The authors thank the following institutions in Argentina: Instituto de Física Aplicada (INFAP-UNSL-CONICET) and Laboratorio de Investigación y Servicios de Química Física (LISeQF-UNSL). The authors also thank Javier Rigau from the Instituto de Investigación en Tecnología Química (INTEQUI-UNSL-CONICET) for their determinations of the FTIR, TGA, and DSC; and Ariel Ochoa from the Laboratorio de Membranas y Biomateriales del INFAP-CONICET-UNSL for their contributions to the mechanical test and water vapor permeability results. This paper is in memoriam of Mariana Gutierrez and Enrique Vega.

Conflicts of Interest: The authors declare no conflicts of interest.

References

1. Cortes, C.N.; Narosky, T. *Cien Caracoles Argentinos*; Ed. Albatros: Buenos Aires, Argentina, 1997.
2. Lasta, M.L.; Ciocco, N.F.; Bremec, C.; Roux, A. Moluscos bivalvos y gasterópodos. *Mar Argent. Sus Recur. Pesq.* **1998**, *2*, 115–142.
3. Carranza, A.; Scarabino, F.; Ortega, L. Distribution of large benthic gastropods in the Uruguayan continental shelf and Río de la Plata estuary. *J. Coast. Res.* **2008**, *24*, 161–168. [[CrossRef](#)]
4. Tsai, W.T.; Yang, J.M.; Lai, C.W.; Cheng, Y.H.; Lin, C.C.; Yeh, C.W. Characterization and adsorption properties of eggshells and eggshell membrane. *Bioresour. Technol.* **2006**, *97*, 488–493. [[CrossRef](#)]
5. Yasothai, R.; Kavithaa, N.V. Chemical characterization of egg shell meal. *Int. J. Sci. Environ. Technol.* **2014**, *3*, 1436–1439.
6. Zaman, T.; Mostari, M.; Mahmood, M.A.A.; Rahman, M.S. Evolution and characterization of eggshell as a potential candidate of raw material. *Cerâmica* **2018**, *64*, 236–241. [[CrossRef](#)]
7. Ajala, E.O.; Eletta, O.A.A.; Ajala, M.A.; Oyeniyi, S.K. Characterization and evaluation of chicken eggshell for use as a bio-resource. *Arid Zone J. Eng. Technol. Environ.* **2018**, *14*, 26–40.
8. Yi, F.; Guo, Z.X.; Zhang, L.-X.; Yu, J.; Li, Q. Soluble eggshell membrane protein: Preparation, characterization and biocompatibility. *Biomaterials* **2004**, *25*, 4591–4599. [[CrossRef](#)]
9. Baláz, M. Eggshell membrane biomaterial as a platform for applications in materials science. *Acta Biomater.* **2014**, *10*, 3827–3843. [[CrossRef](#)]
10. Dinculescu, D.; Gîjiu, C.L.; Apetroaei, M.R.; Isopescu, R.; Rău, I.; Schröder, V. Optimization of chitosan extraction process from Rapanavenosa egg capsules waste using experimental design. *Materials* **2023**, *16*, 525. [[CrossRef](#)]
11. Schröder, V.; Rau, I.; Dobrin, N.; Stefanov, C.; Mihali, C.-V.; Paduretu, C.-C.; Apetroaei, M.R. Micromorphological details and identification of chitinous wall structures in *Rapanavenosa* (Gastropoda, Mollusca) egg capsules. *Sci. Rep.* **2020**, *10*, 14550. [[CrossRef](#)] [[PubMed](#)]
12. Oyekunle, D.T.; Omoleye, J.A. New process for synthesizing chitosan from snail shells. In *Journal of Physics: Conference Series*; IOP Publishing: Bristol, UK, 2019; Volume 1299, p. 012089.
13. Shi, Y.; Zhou, K.; Li, D.; Guyonnet, V.; Hincke, M.T.; Mine, Y. Avian eggshell membrane as a novel biomaterial: A review. *Foods* **2021**, *10*, 2178. [[CrossRef](#)] [[PubMed](#)]
14. Mohan, K.; Muralisankar, T.; Jayakumar, R.; Rajeevgandhi, C. A study on structural comparisons of α -chitin extracted from marine crustacean shell waste. *Carbohydr. Polym. Technol. Appl.* **2021**, *2*, 100037. [[CrossRef](#)]
15. Dahmane, E.M.; Taourirte, M.; Eladlani, N.; Rhazi, M. Extraction and characterization of chitin and chitosan from *Parapenaeus longirostris* from Moroccan local sources. *Int. J. Polym. Anal. Charact.* **2014**, *19*, 342–351. [[CrossRef](#)]
16. Guru, P.S.; Dash, S. Sorption on eggshell waste—A review on ultrastructure, biomineralization and other applications. *Adv. Colloid Interface Sci.* **2014**, *209*, 49–67. [[CrossRef](#)] [[PubMed](#)]
17. Galiano, F.; Briceño, K.; Marino, T.; Molino, A.; Christensen, K.V.; Figoli, A. Advances in biopolymer-based membrane preparation and applications. *J. Membr. Sci.* **2018**, *564*, 562–586. [[CrossRef](#)]
18. Cardenas, G.; Miranda, S.P. FTIR and TGA studies of chitosan composite films. *J. Chil. Chem. Soc.* **2004**, *49*, 291–295. [[CrossRef](#)]
19. Beppu, M.M.; Vieira, R.S.; Aimoli, C.G.; Santana, C.C. Crosslinking of chitosan membranes using glutaraldehyde: Effect on ion permeability and water absorption. *J. Membr. Sci.* **2007**, *301*, 126–130. [[CrossRef](#)]
20. Al Sagheer, F.A.; Al-Sughayer, M.A.; Muslim, S.; Elsabee, M.Z. Extraction and characterization of chitin and chitosan from marine sources in Arabian Gulf. *Carbohydr. Polym.* **2009**, *77*, 410–419. [[CrossRef](#)]
21. Barbosa, H.F.; Francisco, D.S.; Ferreira, A.P.; Cavalheiro, É.T. A new look towards the thermal decomposition of chitins and chitosans with different degrees of deacetylation by coupled TG-FTIR. *Carbohydr. Polym.* **2019**, *225*, 115232. [[CrossRef](#)] [[PubMed](#)]
22. González-Campos, J.B.; Prokhorov, E.; Luna-Bárceñas, G.; Galván, A.M.; Sanchez, I.C.; Donlucas, S.M.N.; Garcia-Gaitan, B.; Kovalenko, Y. Relaxations in chitin: Evidence for a glass transition. *J. Polym. Sci. Part B Polym. Phys.* **2009**, *47*, 932–943. [[CrossRef](#)]
23. Zheng, Y.; Li, X.; Huang, Y.; Li, H.; Chen, L.; Liu, X. Two colorimetric films based on chitin whiskers and sodium alginate/gelatin incorporated with anthocyanins for monitoring food freshness. *Food Hydrocoll.* **2022**, *127*, 107517. [[CrossRef](#)]
24. Kaewmanee, T.; Benjakul, S.; Visessanguan, W. Changes in chemical composition, physical properties and microstructure of duck egg as influenced by salting. *Food Chem.* **2009**, *112*, 560–569. [[CrossRef](#)]
25. Yu, H.; Tang, Q.; Wu, J.; Lin, Y.; Fan, L.; Huang, M.; Lin, J.; Li, Y.; Yu, F. Using eggshell membrane as a separator in supercapacitor. *J. Power Sources* **2012**, *206*, 463–468. [[CrossRef](#)]
26. Park, S.; Choi, K.S.; Lee, D.; Kim, D.; Lim, K.T.; Lee, K.-H.; Seonwoo, H.; Kim, J. Eggshell membrane: Review and impact on engineering. *Biosyst. Eng.* **2016**, *151*, 446–463. [[CrossRef](#)]
27. Jayaraj, K.; Gopi, S.; Rajeswari, A.; Christy, E.J.S.; Pius, A. Microscopic studies on chitin and chitosan-based interpenetrating polymer networks, gels, blends, composites, and nano-composites. In *Handbook of Chitin and Chitosan*; Elsevier: Amsterdam, The Netherlands, 2020; pp. 95–138.
28. Illanes, C.O.; Takara, E.A.; Masuelli, M.A.; Ochoa, N.A. pH-responsive gum tragacanth hydrogels for high methylene blue adsorption. *J. Chem. Technol. Biotechnol.* **2024**, *99*, 31–39. [[CrossRef](#)]
29. Battampara, P.; Sathish, T.N.; Reddy, R.; Guna, V.; Nagananda, G.; Reddy, N.; Ramesha, B.; Maharaddi, V.; Rao, A.P.; Ravikumar, H.; et al. Properties of chitin and chitosan extracted from silkworm pupae and egg shells. *Int. J. Biol. Macromol.* **2020**, *161*, 1296–1304. [[CrossRef](#)] [[PubMed](#)]

30. de Moraes, M.A.; Cocenza, D.S.; da Cruz Vasconcellos, F.; Fraceto, L.F.; Beppu, M.M. Chitosan and alginate biopolymer membranes for remediation of contaminated water with herbicides. *J. Environ. Manag.* **2013**, *131*, 222–227. [[CrossRef](#)] [[PubMed](#)]
31. Chang, X.; Hou, Y.; Liu, Q.; Hu, Z.; Xie, Q.; Shan, Y.; Li, G.; Ding, S. Physicochemical and antimicrobial properties of chitosan composite films incorporated with glycerol monolaurate and nano-TiO₂. *Food Hydrocoll.* **2021**, *119*, 106846. [[CrossRef](#)]
32. Rupiasih, N.N.; Sumadiyasa, M.; Putra, I.K. The effect of variations in the ratio of matrix/solvent on the physical and mechanical properties of chitosan biopolymer membranes. In *IOP Conference Series: Materials Science and Engineering*; IOP Publishing: Bristol, UK, 2017; Volume 196, p. 012039.
33. Baig, U.; Faizan, M.; Waheed, A. A review on super-wettable porous membranes and materials based on bio-polymeric chitosan for oil-water separation. *Adv. Colloid Interface Sci.* **2022**, *303*, 102635. [[CrossRef](#)] [[PubMed](#)]
34. Mamba, F.B.; Mbuli, B.S.; Ramontja, J. Recent advances in biopolymeric membranes towards the removal of emerging organic pollutants from water. *Membranes* **2021**, *11*, 798. [[CrossRef](#)] [[PubMed](#)]
35. Salehi, E.; Daraei, P.; Shamsabadi, A.A. A review on chitosan-based adsorptive membranes. *Carbohydr. Polym.* **2016**, *152*, 419–432. [[CrossRef](#)] [[PubMed](#)]
36. Hardian, R.; Alammar, A.; Holtzl, T.; Szekely, G. Fabrication of sustainable organic solvent nanofiltration membranes using cellulose–chitosan biopolymer blends. *J. Membr. Sci.* **2022**, *658*, 120743. [[CrossRef](#)]
37. Honarkar, H.; Barikani, M. Applications of biopolymers I: Chitosan. *Monatshfte Chem. -Chem. Mon.* **2009**, *140*, 1403–1420. [[CrossRef](#)]
38. Zango, Z.U.; Dennis, J.O.; Aljameel, A.I.; Usman, F.; Ali, M.K.M.; Abdulkadir, B.A.; Algessair, S.; Aldaghri, O.A.; Ibnaouf, K.H. Effective removal of methylene blue from simulated wastewater using ZnO-chitosan nano-composites: Optimization, kinetics, and isotherm studies. *Molecules* **2022**, *27*, 4746. [[CrossRef](#)] [[PubMed](#)]
39. Wan, X.; Rong, Z.; Zhu, K.; Wu, Y. Chitosan-based dual network composite hydrogel for efficient adsorption of methylene blue dye. *Int. J. Biol. Macromol.* **2022**, *222*, 725–735. [[CrossRef](#)] [[PubMed](#)]
40. Wu, S.; Shi, W.; Li, K.; Cai, J.; Xu, C.; Gao, L.; Lu, J.; Ding, F. Chitosan-based hollow nanofiber membranes with polyvinylpyrrolidone and polyvinyl alcohol for efficient removal and filtration of organic dyes and heavy metals. *Int. J. Biol. Macromol.* **2023**, *239*, 124264. [[CrossRef](#)] [[PubMed](#)]
41. Khoerunnisa, F.; Amanda, P.C.; Nurhayati, M.; Hendrawan, H.; Lestari, W.W.; Sanjaya, E.H.; Handayani, M.; Oh, W.-D.; Lim, J. Promotional effect of ammonium chloride functionalization on the performance of polyethersulfone/chitosan composite-based ultrafiltration membrane. *Chem. Eng. Res. Des.* **2023**, *190*, 366–378. [[CrossRef](#)]
42. Heredia-Guerrero, J.A.; Benítez, J.J.; Porras-Vázquez, J.M.; Tedeschi, G.; Morales, Y.; Fernández-Ortuño, D.; Athanassiou, A.; Guzman-Puyol, S. Plasticized, greaseproof chitin bioplastics with high transparency and biodegradability. *Food Hydrocoll.* **2023**, *145*, 109072. [[CrossRef](#)]
43. De Carli, C.; Aylanc, V.; Mouffok, K.M.; Santamaria-Echart, A.; Barreiro, F.; Tomás, A.; Pereira, C.; Rodrigues, P.; Vilas-Boas, M.; Falcão, S.I. Production of chitosan-based biodegradable active films using bio-waste enriched with polyphenol propolis extract envisaging food packaging applications. *Int. J. Biol. Macromol.* **2022**, *213*, 486–497. [[CrossRef](#)] [[PubMed](#)]
44. Yanat, M.; Schroën, K. Advances in chitin-based nanoparticle use in biodegradable polymers: A review. *Carbohydr. Polym.* **2023**, *312*, 120789. [[CrossRef](#)] [[PubMed](#)]
45. Domard, A.; Rinaudo, M. Preparation and characterization of fully deacetylated chitosan. *Int. J. Biol. Macromol.* **1983**, *5*, 49–52. [[CrossRef](#)]
46. Brine, C.J.; Austin, P.R. Chitin variability with species and method of preparation. *Comp. Biochem. Physiol. Part B Comp. Biochem.* **1981**, *69*, 283–286. [[CrossRef](#)]
47. Mohan, K.; Ganesan, A.R.; Ezhilarasi, P.N.; Kondamareddy, K.K.; Rajan, D.K.; Sathishkumar, P.; Rajarajeswaran, J.; Conterno, L. Green and eco-friendly approaches for the extraction of chitin and chitosan: A review. *Carbohydr. Polym.* **2022**, *287*, 119349. [[CrossRef](#)] [[PubMed](#)]
48. Zanon, M.; Masuelli, M. Alcayota Gum Films: Experimental Reviews. *J. Mater. Sci. Chem. Eng.* **2018**, *6*, 11. [[CrossRef](#)]
49. Lazo, L.; Melo, G.M.; Auad, M.L.; Filippa, M.; Masuelli, M.A. Synthesis and characterization of Chañar gum films. *Colloids Interfaces* **2022**, *6*, 10. [[CrossRef](#)]
50. Saheed, I.O.; Da Oh, W.; Suah, F.B.M. Chitosan modifications for adsorption of pollutants—A review. *J. Hazard. Mater.* **2021**, *408*, 124889. [[CrossRef](#)] [[PubMed](#)]
51. da Silva Alves, D.C.; Healy, B.; Pinto, L.A.D.A.; Cadaval Jr, T.R.S.A.; Breslin, C.B. Recent developments in chitosan-based adsorbents for the removal of pollutants from aqueous environments. *Molecules* **2021**, *26*, 594. [[CrossRef](#)] [[PubMed](#)]
52. Scudeler, C.G.D.S.; Costa, T.D.L.; Cortez-Vega, W.R.; Prentice, C.; Fonseca, G.G. Development and characterization of Nile tilapia (*Oreochromis niloticus*) protein isolate-based biopolymer films incorporated with essential oils and nanoclay. *Food Packag. Shelf Life* **2020**, *25*, 100542. [[CrossRef](#)]
53. Ruano, P.; Delgado, L.L.; Picco, S.; Villegas, L.; Tonelli, F.; Merlo, M.E.A.; Rigau, J.; Diaz, D.; Masuelli, M. Extraction and characterization of pectins from peels of Criolla Oranges (*Citrus sinensis*): Experimental reviews. In *Pectins-Extraction, Purification, Characterization and Applications*; INTECH Publishing: Rijeka, Croatia, 2020; pp. 1–45.
54. Bielska, M.; Szymanowski, J. Removal of methylene blue from waste water using micellar enhanced ultrafiltration. *Water Res.* **2006**, *40*, 1027–1033. [[CrossRef](#)]

-
55. Masuelli, M.A. Ultrafiltration of oil/water emulsions using PVDF/PC blend membranes. *Desalination Water Treat.* **2015**, *53*, 569–578. [[CrossRef](#)]
 56. Masuelli, M.A. Synthesis polysulfone-acetyethanol ultrafiltration membranes. Application to oily wastewater treatment. *J. Mater. Phys. Chem.* **2013**, *1*, 37–44.

Disclaimer/Publisher’s Note: The statements, opinions and data contained in all publications are solely those of the individual author(s) and contributor(s) and not of MDPI and/or the editor(s). MDPI and/or the editor(s) disclaim responsibility for any injury to people or property resulting from any ideas, methods, instructions or products referred to in the content.